Spectroscopic and Functional Characterization of T State Hemoglobin Conformations Encapsulated in Silica Gels†

Uri Samuni,‡ David Dantsker,‡ Laura J. Juszczak,‡ Stefano Bettati,§ Luca Ronda,|| Andrea Mozzarelli,|| and Joel M. Friedman*,‡

Physiology and Biophysics, Albert Einstein College of Medicine, 1300 Morris Park Avenue, Ullman 303, Bronx, New York 10461, and Department of Public Health, University of Parma, Via Volturno 39, and Department of Biochemistry and Molecular Biology, University of Parma, Parco Area delle Scienze 23/A, 43100 Parma, Italy

Received July 11, 2004; Revised Manuscript Received August 26, 2004

ABSTRACT: Oxygen binding curves of sol−gel-encapsulated deoxy human adult hemoglobin (HbA) have previously revealed two distinct noncooperative populations with oxygen binding affinities approximately 1000 and 100 times lower than that of the high-affinity R state. The two populations which have been termed the low-affinity (LA) and high-affinity (HA) T states can be selectively stabilized using two different encapsulation protocols for deoxy-HbA. The present study seeks to understand the factors giving rise to these different affinity states. Visible and UV resonance Raman spectroscopies are used to characterize the conformational properties of both the deoxy and deoxy-turned-carbonmonoxy (CO) derivatives of HbA derived from the two encapsulation protocols. The geminate and bimolecular recombination of CO to the photodissociated CO derivatives is used to characterize the functional properties of the slowly evolving encapsulated populations. The results show that the initial deoxy-HbA populations are conformationally indistinguishable with respect to encapsulation protocol. The addition of CO to sol−gel-encapsulated deoxy-HbA triggers a detectable progression of conformational and functional changes. Visible resonance Raman spectra of the CO photoproduct reveal a progression of changes of the iron-proximal histidine stretching frequencies: 215, 222, 227, and 230 cm^{-1}. The low and high values correspond to the initial deoxy T state and liganded R (R_2) state species, respectively. The 222 and 227 cm^{-1} species are generated using encapsulation protocols that give rise to what are termed the LA and HA T states, respectively. The UV resonance Raman spectra of these and related species indicate that the progression from deoxy T to LA to HA is associated with a progressive loosening of T state constraints within the hinge and switch regions of the $\alpha_1\beta_2$ interface. The time scale for the progression is determined by a balance between the ligation-initiated evolution toward high-affinity conformations and factors such as allosteric effectors, gel matrix, and added glycerol that slow ligand-binding-induced relaxation. Thus, it appears that the encapsulation protocol-dependent rate of ligand-binding-induced relaxation determines the functional properties of the initially encapsulated deoxy-HbA population.

The cooperative binding of ligands to the hemoglobin tetramer is accompanied by a transition of the structure of the protein from the low-affinity, unliganded T quaternary configuration to the high-affinity, ligand saturated R quaternary configuration. The sequence and nature of the ligation-induced structural transitions linking these two end point functional states are not fully understood especially with regard to the mechanism of cooperativity (*1*, *2*). Recent studies have suggested that human adult hemoglobin (HbA)[1] can exhibit a larger degree of conformational and functional plasticity than what is accepted under the traditional two-state model (*3*). Crystallography (*4*) and NMR (*5*) studies show clear evidence for multiple R state conformations. Moreover, thermodynamic (*6*, *7*), functional (*8*−*10*), and spectroscopic (*10*) studies reveal indications of functionally distinct T state species. Furthermore, the traditional view that the role of effectors in modulating ligand affinity arises exclusively from an effector-induced shift in the equilibrium between the two quaternary structures is being reassessed due to more recent studies indicating that effectors can modulate the tertiary structure and functionality within a given quaternary state including both the R and T states (*11*, *12*). Recently, a tertiary two-state allosteric model has been proposed that explains the functional variability by distinct populations of tertiary t and r conformations within the quaternary T and R states (*13*).

† Financial support for this study was provided by Grant P01 GM58890 to J.M.F. and A.M. and FIRB Nanotechnologies 2003 to A.M.

* To whom correspondence should be addressed. Phone: (718) 430-3591. Fax: (718) 430-8819. E-mail: jfriedma@aecom.yu.edu.

‡ Albert Einstein College of Medicine.

§ Department of Public Health, University of Parma.

|| Department of Biochemistry and Molecular Biology, University of Parma.

[1] Abbreviations: HbA, human hemoglobin A; LA, low affinity; HA, high affinity; IHP, inositol hexaphosphate; BZF, bezafibrate; TMOS, tetramethyl orthosilicate; L35, 2-[4-({[(3,5-dichlorophenyl)amino]-carbonyl}amino)phenoxy]-2-methylpropanoic acid; VRR, visible resonance Raman; UVRR, UV resonance Raman spectra; CW, continuous wave; NMR, nuclear magnetic resonance; CD, circular dichroism.

10.1021/bi048531d CCC: $27.50
Published on Web 10/05/2004

The mapping out of the sequence of conformational changes associated with the quaternary transition and the functional importance of the various intermediates are key objectives with regard to developing a detailed molecular level understanding of cooperativity. Studying this sequence of structural transitions is an inherently difficult task as the species involved are often short-lived intermediates, making spectroscopic and functional characterization difficult. Time-resolved spectroscopy, including absorption (*14*−*18*), CD (*19*), visible resonance Raman (*20*−*22*), and UV resonance Raman (*23*−*25*) have been successful in mapping out some of the conformational changes occurring after rapid ligand photodissociation in solution. Those approaches are typically limited to those conformational transitions initiated through ligand dissociation. Furthermore, in solution, functional characterization of intermediates becomes virtually impossible since the relaxation times of the nonequilibrium populations are too fast to allow for functional characterization using ligand affinity measurements. Thus, to a great extent, the limitations associated with solution-phase studies of both ligand-binding-induced changes and functional properties of intermediates arise from ligand diffusion times that are much slower than the lifetime of allosteric intermediates.

The novel approach of sol−gel encapsulation of proteins (*26*, *27*) breaks this "diffusion barrier" since the gel environment can slow conformational change to a degree where it is much slower than ligand diffusion times. A major advantage is that sol−gel-encapsulated biomolecules are still solvated, allowing for direct comparisons with solution-based studies. Indeed, previous studies have demonstrated that sol−gel encapsulation of myoglobin (Mb) (*28*−*32*) and Hb (*8*, *30*, *32*−*39*) does not perturb structural and functional properties of individual tertiary and quaternary states. Nevertheless, under the appropriate conditions, encapsulation effectively prevents the interconversion of conformational states in Mb (*30*) and pyridoxal 5′-phosphate-dependent enzymes (*40*).

Early studies on sol−gel-encapsulated deoxy-HbA showed that the encapsulated HbA bound oxygen noncooperatively, with a low affinity consistent with T state properties (*33*, *37*). The CO rebinding kinetics of encapsulated deoxy-HbA samples exposed to CO were similarly consistent with T state properties (*10*, *36*, *41*, *42*). Most recently, it was shown that deoxy-HbA encapsulated using two different protocols binds oxygen noncooperatively but with protocol-specific affinities (*8*). In both cases the oxygen affinity is distinctly lower than that associated with an encapsulated R state population (e.g., encapsulated O_2HbA, P_{50} of 0.16 mmHg (*37*)). The two encapsulated populations have been referred to as low-affinity (LA) T and high-affinity (HA) T, on the basis of the assumption that in both cases the sol−gel matrix prevents the T → R transition upon oxygen binding during the time course of the affinity measurements (*8*). Other encapsulation studies have also yielded indications of T state populations with different oxygen affinities (*9*). It is remarkable that LA exhibits the same oxygen affinity as T state HbA crystals (*43*, *44*).

The present study seeks to further characterize these LA and HA populations with the intent of exposing those factors responsible for the different oxygen binding affinities. Visible (Soret-enhanced) and UV resonance Raman spectroscopies

Scheme 1

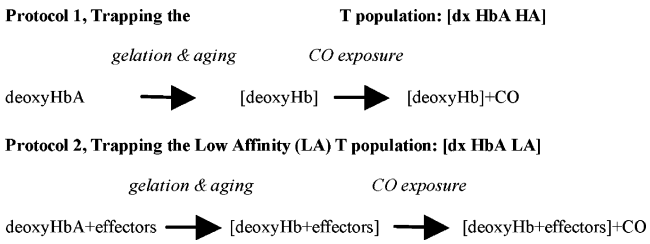

are used to characterize the deoxy-HbA samples encapsulated using the LA and HA protocols. The response of the LA and HA deoxy-HbA samples to ligand binding is explored by exposing the samples to CO. Visible Resonance Raman (VRR) spectroscopy of the 8 ns photoproduct of the deoxy-turned-CO samples is used to probe the response of the heme environment to CO-binding-induced conformational changes (*22*, *45*). UVRR spectroscopy (excitation at 229 nm) is utilized to probe CO-binding-induced structural changes in the $\alpha_1\beta_2$ interface, utilizing the position and shape of specific tryptophan and tyrosine bands which are known quaternary and tertiary structure markers (*23*, *24*, *46*−*49*). The functional properties of LA and HA deoxy-turned-CO samples were followed using CO recombination (including geminate and solvent phases) after photodissociation using an 8 ns photodissociation pulse (*36*, *41*, *42*). Our results show that the two samples generated by adding CO to deoxy-HbA encapsulated in the two protocols have distinctly different spectroscopic and kinetic signatures, and expose the role of effectors in controlling the relaxation properties of T state populations of HbA under nonequilibrium conditions.

MATERIALS AND METHODS

Materials. All materials, including inositol hexaphosphate (IHP), bezafibrate (BZF), and tetramethyl orthosilicate (TMOS) were commercially obtained at the highest purity available. 2,[4-({[(3,5-dichlorophenyl)amino]carbonyl}amino)-phenoxy]-2-methylpropanoic acid (L35) (*50*) was obtained as a gift from Dr. I. Lalezari. Human hemoglobin was purified as described previously (*43*).

Sol−*Gel Encapsulation.* Two different previously described (*8*) preparative protocols were used, designed to prepare the two different affinity T states (or populations) of HbA: HA and LA T states. When referring to the samples, we use a notation that indicates the history of the samples (see Scheme 1). Square brackets are used to indicate the species and conditions present during the sol−gel encapsulation and aging. Any changes to the samples after gelation and aging (e.g., the addition of a ligand or a change in bathing buffer) appear outside and to the right of the square brackets with subsequent modifications added on the right. To allow comparison of this study with the previous affinity and kinetic measurements on the HA and LA T states (*8*), we have employed the exact same sample preparation protocols (*8*), where the HA and LA protocols correspond, respectively, to protocols 1 and 2 in that paper as well as in Scheme 1. All the buffers and solutions were deoxygenated prior to gelation, and the deoxy-HbA stock was generated by nitrogen purging and reduction with dithionite. Anaerobic conditions were kept at all steps prior to CO addition. UV/vis measurements were taken before and after gelation to verify that the samples are deoxy and that no binding to oxygen or any

change in the oxidation state of the iron occurred during the procedure. The sample made in the low-affinity protocol (protocol 2), labeled [dx HbA LA], had effectors present during gelation (2 mM bezafibrate, 2 mM IHP, and 50 mM phosphate). The bathing buffer contained all the effectors but was either 100 mM phosphate and 1 mM EDTA, pH 7.0, or 50 mM BisTris, 50 mM Tris, 200 mM chloride, and 1 mM EDTA, pH 7.0. Samples made in the high-affinity protocol (protocol 1), labeled [dx HbA HA], had no effectors present during the gelation, and the bathing buffer was 100 mM Hepes, pH 7.0, and 1 mM EDTA. The final protein concentration in the sol−gel samples was ~0.5 mM in heme.

For both protocols the gels were cast on the inner bottom surface of an NMR tube (Wilmad, Buena, NJ, or New Era Enterprises, Vineland, NJ). A thin film was obtained by rapidly spinning the NMR tube using a tube spinner (Princeton Photonics, Princeton, NJ). After gelation was complete, the gels were washed several times and then filled with excess buffer (phosphate buffer or Tris buffer both with effectors for the LA samples, and effector-free Hepes buffer for the HA samples) and left to age at 4 °C for a minimum of 2 days. It should be noted that the method of gel casting in this study is different from the one used in the work by Mozzarelli and co-workers (*8*). The variation of the casting method proved to be inconsequential as the oxygen affinity measurements of the generated HA T and LA T samples reproduced the results of the previous study (data not shown).

Experimental Procedure. To improve "locking in" and minimize the relaxation of nonequilibrium populations trapped within the sol−gel, the samples were always kept at ~4 °C. The "clock" is started by a rapid addition of CO to the sol−gel-encapsulated samples. CO binding to the heme is monitored using UV/vis spectra. Usually within 5 min the sample turns fully CO. Then the samples are measured on the UVRR setup, VRR setup, and kinetic setup (CO rebinding by way of transient absorption).

Experimental Protocols for VRR, UVRR, and CO Rebinding. 1. Visible Resonance Raman Spectroscopy. VRR spectra were generated using an 8 ns pulsed laser at 435.8 nm (obtained using a hydrogen-filled Raman cell to Raman shift 532 nm pulses of a Nd:YAG laser (Continuum, Santa Clara, CA)). The NMR tubes were spun and cooled (~4 °C). A detailed description is available elsewhere (*10*, *29*, *51*).

2. UV Resonance Raman spectroscopy. UVRR spectra were generated using a continuous wave (CW) laser at 229 nm as described previously (*10*, *35*). The sample-containing NMR tubes were cooled (~4−10 °C) and both spun and restored vertically to minimize sample heating and laser-induced degradation. The absorption spectrum of the sample was recorded before and after each UVRR measurement.

3. CO Rebinding Kinetics. CO recombination measurements were carried out by following the transient absorption of the sample. Pulses of 8 ns duration at 532 nm and 1 Hz from a Nd:YAG laser (Minilite, Continuum) were used for the CO photodissociation. A greatly attenuated CW laser at 442 nm was used as the probe. Samples were kept at 3.5 °C. A detailed description is available elsewhere (*51*, *52*).

RESULTS

VRR Spectra. The VRR spectra of the sol−gel-encapsulated, fully deoxy-HbA species, are essentially identical to that of solution-phase deoxy-HbA (trace not shown). In addition, the spectra are the same for deoxy samples encapsulated using either the LA or the HA protocol (see Figure 1a). Once CO was added to the samples and bound to the heme (as reflected in the visible absorption spectrum), ligation-induced conformational changes in the heme environment were evident in the 8 ns photoproduct VRR spectrum. These changes are qualitatively similar to those that are typically observed when deoxy-Hb evolves to HbCO derivatives (*21*, *22*, *45*). These include an increase in frequency of ν(Fe−His), a loss of intensity for the 341 cm^{-1} band (ν_8), and an upshift in the 300 cm^{-1} γ_7 band.

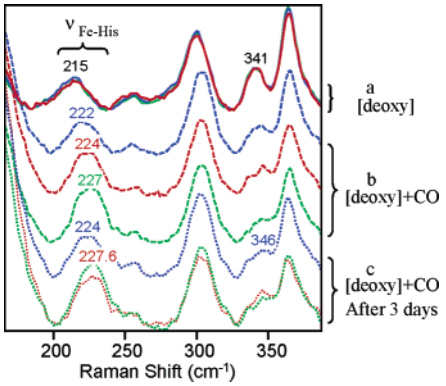

FIGURE 1: Low-frequency region of the VRR spectra of HbA HA and LA gels. All the samples were made in the gel as deoxy. The traces of the various samples are color coded; LA is blue, HA is green, and an LA sample where the BZF effector was washed off is red. Panel a shows the VRR spectra of the deoxy species. Panel b shows the VRR spectra of the 8 ns photoproducts of the same samples immediately after they were converted to the CO derivative. Panel c shows the VRR spectra of the 8 ns photoproducts of the same samples 3 days after they were converted to the CO derivative. The spectra were normalized to the ν_7 peak.

In contrast to the encapsulated deoxy-Hb samples whose VRR spectra are independent of encapsulation protocols, the deoxy-turned-HbCO samples display protocol-sensitive VRR spectra for the 8 ns photoproduct immediately (within 1 h) after CO ligation. In particular, the frequency of ν(Fe−His) differs for the initial photoproduct spectrum of the HA and LA samples. The visible resonance Raman spectra of the photoproduct of [dx HbA LA] + CO (i.e., sol−gel-encapsulated CO-ligated HbA, which was initially encapsulated and aged as deoxy-HbA in the presence of effectors following protocol 2), measured shortly after CO addition, revealed a ν(Fe−His) band with a frequency of 222 cm^{-1}. This rapid increase in the Fe−His frequency from that of [dx HbA + effectors] at 214 cm^{-1} (i.e., the same sample before CO addition) shows that some conformational relaxation has occurred. The visible resonance Raman spectra of the photoproduct of [dx HbA HA] + CO (i.e., sol−gel-encapsulated CO-ligated HbA, which was initially encapsulated and aged as deoxy-HbA following protocol 1), again measured shortly after CO addition, revealed a ν(Fe−His) band with an even higher frequency of 227 cm^{-1}. Thus, for the HA encapsulation protocol, the ν(Fe−His) frequency for the 8 ns photoproduct is at a higher frequency, indicating that there is an almost immediate (on the time scale of the measurements) ligand-binding-induced relaxation for the HA sample that is substantially greater than for the corresponding LA sample (see Figure 1b).

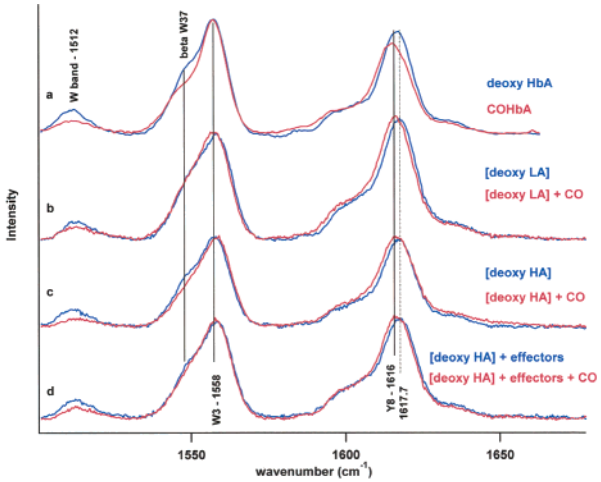

FIGURE 2: UV resonance Raman spectra of sol−gel-encapsulated deoxy-HbA samples before and after CO addition. All the samples were made in the gel as deoxy. Traces are color coded. For the sol−gel samples, deoxy samples are blue, while red is used for the same samples after CO was added. The measurements for the latter samples were taken immediately after CO addition. Panel a displays, as a reference, the spectra of solution samples of deoxy-HbA and CO-ligated HbA. Panel b is for the LA sample. Panel c is for the HA sample. Panel d is for an HA sample to which effectors (IHP + BZF) were added prior to CO addition. The excitation laser was at 229 nm.

Figure 1 also displays a third sample prepared using a modified version of protocol 2 used for LA, where the potential potency of the effectors has been reduced by removing BZF following gelation and aging ([dx HbA LA] − BZF). The unliganded deoxy-HbA gel of this sample gives the same VRR spectra as the other two gels (Figure 1a) with the same frequency for ν(Fe−His). However, the VRR spectrum of the photoproduct of the CO-liganded sol−gel-encapsulated deoxy-HbA in the absence of BZF, measured immediately after CO addition ([dx HbA LA] − BZF + CO), reveals a ν(Fe−His) frequency of 224 cm^{-1} (Figure 1b), indicative of an intermediate degree of conformational relaxation compared to that of the standard HA and LA samples.

UVRR Spectra. The UVRR spectra of the encapsulated deoxy-HbA samples (Figure 2) are all very similar to that of the corresponding deoxy-HbA in solution. The comparison of the UVRR spectra before and immediately after CO addition shows shifts in the Y8 band position at ∼1617 cm^{-1} for both the HA and LA samples. This behavior parallels that observed for HbA in solution where the ligation-induced 2 cm^{-1} shift in this band is associated with the disruption of the α42Y-β99D T state hydrogen bond in the "switch" region of the $\alpha_1\beta_2$ interface upon relaxation to the R state (*47*, *49*, *53*). In contrast, the intensity of the β37 tryptophan shoulder of the W3 band, a sensitive marker for the status of the hinge region of the $\alpha_1\beta_2$ interface, decreases for the HA sample (in the direction of the liganded R state) but not for the LA sample or the HA sample to which effectors were added. Furthermore, the CO-binding-induced intensity change for the β37 tryptophan-sensitive band at 1512 cm^{-1} (also a marker of the hinge region) (*29*, *54*) is more prominent for the HA sample but less than that for solution-phase samples. Both markers indicate that the HA sample has relaxed away more extensively from the deoxy T state compared to the LA sample.

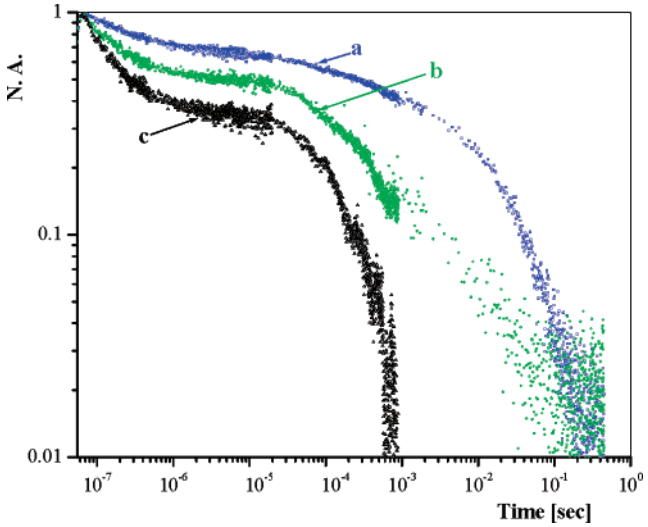

FIGURE 3: CO rebinding kinetics of sol−gel-encapsulated HbA: trace a, [dx HbA LA] + CO; trace b, [dx HbA HA] + CO; trace c, [CO HbA]. All measurements were done at 3.5 °C. Traces a and b were measured immediately after the addition of CO to the deoxy gels.

It is interesting to note that when effectors were added to an aged deoxy HA sample, the UVRR spectroscopic markers of that sample, when measured immediately after CO ligation, behave more like the LA sample with an amplitude reduction in the changes in the hinge region markers (see Figure 2c).

CO Rebinding Kinetics. Transient absorption measurements, which follow CO rebinding, were measured for CO-liganded samples of sol−gel-encapsulated deoxy-HbA, made via the two different protocols. The species probed in the transient absorption correspond to those probed in the structural measurements (VRR and UVRR) since the kinetic measurements were made on the same samples shortly after the VRR and UVRR measurement (immediately following CO addition).

The CO rebinding measurements correlate well with the spectral and structural results, revealing that the two sample preparation protocols yield samples that exhibit different rebinding kinetics, which are also different from that of a sample trapped in the R state, [CO HbA]. Figure 3 shows a progression of functional properties, as reflected in a decreasing geminate yield in the order [COHbA], [dx HbA HA] + CO, and [dx HbA LA] + CO.

Time Evolution of the Encapsulated Deoxy-Turned-CO Samples. As noted above, the addition of CO to the HA and LA deoxy samples yields spectra that indicate that some relaxation has occurred within a relatively short period of time after the addition of CO. The time course of the structural relaxation is probed by monitoring the VRR spectra of the evolving sample. Figure 1c shows that, 3 days after the CO addition, the values of the ν(Fe−His) frequency for the LA and LA − BZF samples have continued to increase to 224 and 227 cm^{-1}, respectively. The HA sample has increased very slightly to 228 cm^{-1}. Note that even though relaxation continues out to 3 days there are still differences in the spectra when the LA and HA samples are compared.

Following the evolution of the spectra well beyond the initial 3 days reveals that the HA sample does not evolve much more, with the ν(Fe−His) frequency having stabilized

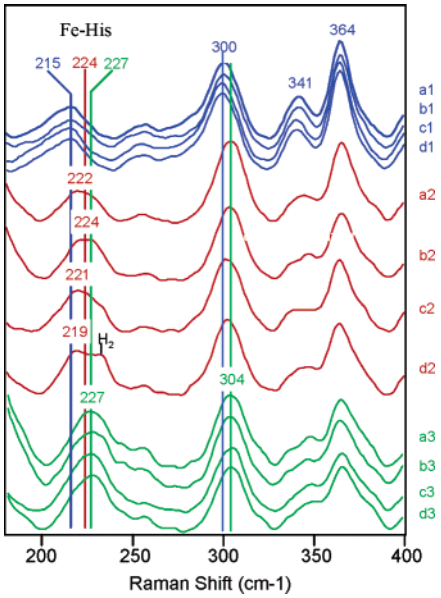

FIGURE 4: VRR spectra of deoxy-HbA samples encapsulated and aged in the sol−gel and their time evolution following CO addition, as a function of the conditions and time. The top four traces show the VRR of the sol−gel-encapsulated deoxy samples: a1, [dx HbA LA]; b1, [dx HbA LA] − BZF; c1, [dx HbA LA] + 50% glycerol − BZF; d1, [dx HbA HA] + 50% glycerol. Traces a2, b2, c2, and d2 show the VRR spectra of the photoproduct of the respective sol−gel samples a1−d1 immediately after CO addition. Traces a3, b3, c3, and d3 show the VRR spectra of the 8 ns photoproduct of the respective sol−gel samples a1−d1 30 days or more after CO addition. The spectra were normalized to the ν_7 band. The peak marked as "H_2" is an artifact due to hydrogen rotational lines originating from the Raman converter cell.

at 227−228 cm^{-1}. The LA samples on the other hand continued to evolve, ending with an Fe−His value of 227 cm^{-1}, very similar to that obtained for the HA sample immediately after CO addition (see Figure 4, trace a3).

The [dx HbA LA] − BZF + CO sample, which showed an intermediate conformational relaxation behavior at early times (see Figure 4, trace b2), reached the same end value for the Fe−His frequency of 227 cm^{-1} measured at 3 days with no further evolution 8 days and 8 months after CO addition (Figure 4, trace b3). Interestingly, the acceleration of the relaxation due to the effect of removing BZF from the LA sample can be reversed when 50% glycerol is added to the bathing buffer. The resonance Raman spectra of the photoproduct of such a sample, [dx HbA LA] − BZF + 50% glycerol + CO measured just after CO addition displayed an Fe−His frequency of 221 cm^{-1}, similar to the LA sample in the presence of BZF ([dx HbA LA] + CO) (Figure 4, traces c2 and a2, respectively). The [dx HbA LA] − BZF + 50% glycerol + CO sample also evolved with time, and after 30 days, the ν(Fe−His) frequency had also reached 227 cm^{-1} (see Figure 4, trace c3).

The ability of added glycerol in the bathing buffer to slow the conformational relaxation is even more pronounced for an HA sample for which the bathing buffer is replaced with a buffer containing 50% glycerol prior to addition of CO. The VRR of the photoproduct of [dx HbA HA] + 50% glycerol + CO measured immediately after CO addition exhibited a very low ν(Fe−His) frequency of 219 cm^{-1}. Interestingly, this frequency, measured in the absence of effectors, is actually lower than that observed for an LA

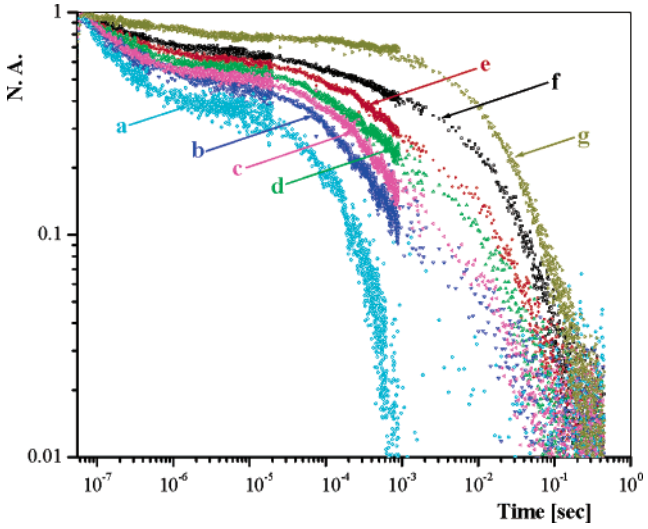

FIGURE 5: CO rebinding kinetics of sol−gel-encapsulated HbA: trace a, [dx HbA HA] + CO 60 days after CO addition; trace b, [dx HbA LA] + CO 44 days after CO addition; trace c, [dx HbA LA − BZF] + CO 8 days after CO addition; trace d, [dx HbA LA] + CO 9 days after CO addition; trace e, [dx HbA LA − BZF] + CO 1 day after CO addition; trace f, [dx HbA LA] + CO 1 day after CO addition; trace g, [dx HbA + IHP + L35] + CO immediately after CO addition. The latter sample was encapsulated using a no sonication protocol (*30*). All measurements were done at 3.5 °C.

sample (222 cm^{-1}) which does contain effectors (see Figure 4, traces d2 and a2, respectively). Despite the low frequency of the initial liganded sample, the high-viscosity HA sample does eventually relax, and after 30 days, the ν(Fe−His) frequency of the photoproduct of [dx HbA HA] + 50% glycerol + CO has also reached 227 cm^{-1} (Figure 4, trace d3).

The CO-initiated relaxation of the HA sample can also be slowed through the addition of effectors (IHP + BZF). It is observed that, when effectors are added to a [dx HbA HA] sample and the resulting sample is allowed to age prior to the addition of CO, the VRR photoproduct spectrum recorded immediately after CO addition shows a low ν(Fe−His) frequency of 221 cm^{-1}, which is similar to that from the protocol 2, LA samples (trace not shown).

Kinetic Behavior as a Function of the Conditions and Time Evolution of the Samples. Figure 5 depicts kinetic traces of CO rebinding to HbA sol−gel samples initially encapsulated as deoxy-Hb using different protocols and then allowed to evolve after the CO addition, for varying lengths of time (up to 60 days from the initial addition of CO to the deoxy samples). Trace a shows the rebinding kinetics of CO to [dx HbA HA] + CO 63 days after CO was added to the deoxy gel. It can be seen that this trace exhibits the highest geminate yield and the most rapid bimolecular rebinding. After more than 60 days, the trace from the HA sample resembles that of [CO HbA] (trace not shown), indicating the protein structure has relaxed considerably toward the end point liganded R state conformation. Traces f, d, and b show the time evolution of the CO rebinding kinetics of [dx HbA LA] + CO from 1 day, 9 days, and 44 days (respectively) after CO was added to the deoxy gel. There is a clear gradual increase in the geminate yield as well as in the rate of the bimolecular rebinding. Traces e and c show the time evolution of the CO rebinding kinetics of [dx HbA LA] −

BZF + CO 1 day and 9 days, respectively, after CO was added to the deoxy gel. Again, there is a gradual increase in the geminate yield as well as in the rate of the bimolecular rebinding. The last trace, g, displays what is close to the limiting end point kinetic trace with respect to reduced geminate yield and a slow bimolecular phase that is very similar to what is measured in CO combination experiments for deoxy-HbA in solution. The sample in trace g, [dx HbA + IHP + L35] + CO, measured shortly after CO addition, was made using a different encapsulation protocol (*30*) that has been shown to be especially effective in limiting (i.e., slowing) ligation-induced relaxation in hemoglobins and myoglobin.

DISCUSSION

Comparing Sol−Gel and Solution Results. A prerequisite to the analysis and discussion of the implication of the sol−gel study is a verification of the assumption that the sol−gel encapsulation does not perturb the native structure of the protein in any significant way, thereby making the results from the sol−gel study applicable to the interpretation of solution-based studies. Indeed, it is known that sol−gel-encapsulated proteins are fully solvated since the gel allows for the free and rapid diffusion of many water-soluble molecules and for the retention of water-dependent protein activity (*55*, *56*). In addition, spectroscopic evidence indicates that the encapsulated equilibrium populations of hemoglobins and myoglobins typically retain the same conformational distribution as in solution (*30*). However, due to the variable nature of the different sol−gel preparation protocols, the implicit assumption that the protein conformation is minimally perturbed by encapsulation must be verified for each new variation of the encapsulation protocol. It has already been shown that the HbA samples encapsulated using the two gelation protocols employed in this study have a "normal" UV/vis absorption spectrum (*8*). Our spectroscopic characterization of the deoxy-HbA sol−gel-encapsulated samples, both HA and LA protocols, show that both the visible resonance Raman and the UV resonance Raman spectra of the sol−gel-encapsulated deoxy-HbA samples are very similar to that of the solution-phase deoxy-HbA, demonstrating that there is little perturbation of the tertiary and quaternary conformation of deoxy-HbA by the sol−gel environment.

Furthermore, the finding that the VRR spectra of deoxy-HbA gels made using the two protocols, as well as for samples where the bathing buffer was later modified (by removal or addition of effectors, or a change of bathing buffer to one containing 50% glycerol), are practically the same (including the frequency of ν(Fe−His)) indicates that the starting structure for all the sol−gel-encapsulated deoxy samples is the same "end point" T structure. We use the expression "end point" since the spectra derived from these samples represent for HbA one limit (on the T state side of the distribution) of the range of accessible conformational populations that are spectroscopically distinct. For Hb the frequency of ν(Fe−His), a spectroscopic marker of the degree of proximal strain, ranges from ∼214 cm^{-1} for deoxy-HbA ± effectors to ∼230 cm^{-1} for the 8 ns photoproduct of the fully liganded R state in the absence of effectors (*21*, *45*, *57*−*60*). The significance of the observation that the LA and HA protocols yield essentially the same end point deoxy-HbA spectrum is that the conformational basis for the functional differences between these two samples must become manifest *only after ligand binding*.

Comparison of the HA and LA Samples. The main objective of the present study was to identify spectroscopic markers that correlate with the two different noncooperative oxygen affinity populations of HbA that were isolated using the HA and LA encapsulation protocols (*8*). Our spectroscopic measurements reveal distinct differences between HA and LA samples associated only with the liganded derivatives. The visible Raman spectra of the photoproduct of LA and HA HbA generated shortly after CO addition to the deoxy gels reveal a difference in the value of the Fe−His frequency, 222 cm^{-1} vs 227 cm^{-1}, respectively. The difference in the ν(Fe−His) frequency for the LA and HA species implies a different proximal environment for the structures of the two intermediate species (or populations), where the conformation of the LA intermediate is closer to that of the initial deoxy T state and that of the HA intermediate is further relaxed toward that of liganded R. The UVRR findings support the VRR findings showing that, following the CO addition, the T state $\alpha_1\beta_2$ interface is more disrupted for the HA sample than for the LA sample, which is consistent with the HA intermediate undergoing more ligation-induced relaxation away from the original end point T state conformation of the starting deoxy-HbA population. The CO rebinding kinetics show that the HA and LA populations have different functional activities, with the CO-saturated LA population exhibiting rebinding kinetics that are closer to those associated with populations that are viewed as extreme T, such as partially liganded iron−metal hybrid forms in the presence of allosteric effectors (*10*).

Conclusions Related to Sample Evolution with Time and Environmental Conditions. Our results, both spectroscopic and kinetic, indicate that the properties of the intermediate species generated upon CO ligation can be modulated by adding or removing effectors after gelation but prior to the addition of CO. This observation is an indication that effectors can not only diffuse in and out of the sol−gel but also bind or detach in a functional manner to the sol−gel-encapsulated protein. This conclusion has implications for sol−gel-based studies as it increases the scope and variety of experiments that can be attempted as well as underlines the precautions that need to be taken to maintain a functional presence of effectors or other small molecules.

An implication derived from the HA and LA study is that the fate of these samples can be modified beyond the initial limitation of the gelation protocol used. The effect of increasing the viscosity of the bathing buffer, where the presence of 50% glycerol greatly slows the conformational relaxation following CO addition, further validates this conclusion (*32*).

The results of the kinetic measurements show that with time there is a considerable evolution of the samples where the kinetic traces progress toward increased geminate yield and faster bimolecular rebinding. The ν(Fe−His) spectroscopic marker also evolves with time, correlating with the functional findings, a result that is consistent with a conformational relaxation away from the initial end point T state conformational population that was initially prepared in the gel. The HA and LA samples start at the same point conformationally/spectroscopically prior to the addition of

CO and *eventually* end up at roughly the same point after the addition of CO. The major difference is the rate at which the populations evolve.

The interpretation that has emerged is that the HA and LA populations result from environmental differences arising from factors including gelation protocol, added effectors, and added glycerol that modulate the relaxation properties of encapsulated deoxy samples upon ligand binding. There is a combination of opposing forces influencing the hemoglobin molecule. The initial binding of CO to the heme generates a nonequilibrium population of CO-liganded HbA. As a result of the ligand binding there is a driving force toward conformational relaxations of the HbA structure leading to the equilibrium COHbA R state structure. On the other hand, there are forces that either favor the deoxy-HbA structure (the binding of effectors) or slow both tertiary and quaternary conformational relaxation (the sol−gel environment, and increased glycerol in the bathing buffer). The net balance between these opposing factors will determine the rate of evolution. In this framework, the relationship between the LA and HA HbA intermediate conformational distribution is that of two points on a path from the end point T state (the initial deoxy-HbA structure) toward the R state (COHbA equilibrium structure). Immediately after CO addition, the HA intermediate has undergone faster conformational relaxation than the LA intermediates, primarily because the relaxation for the LA sample is slowed by the presence of effectors. With time both samples will continue to relax, albeit slowly, due to the sol−gel environment. The structural and functional probes used in the present study support the concept that eventually the HA and LA samples reach a similar stable or quasi stable high-affinity end point (e.g., the frequency of ν(Fe−His) of the photoproduct of the LA sample slowly reaches 227 cm^{-1}, the same value that the HA sample had almost immediately after CO addition).

The above assessment of the origin of the difference in CO reactivity between the HbA populations prepared using the HA and LA protocols can also account for the protocol-specific difference in the oxygen affinity. Oxygen affinity is determined largely by the oxygen dissociation rate, which is a function of the local conformation of the oxygenated protein. On the limited time scale for oxygen titration measurements, the LA sample, relative to the HA sample, will undergo a much more limited conformational shift away from the end point deoxy T state population upon binding of dioxygen. As a result, the dissociation rate for the LA oxygenated heme is anticipated to be higher than for the hemes in the HA samples. On the basis of the CO-induced behavior, oxygenation for the HA sample should rapidly induce a much more extensive (vis-à-vis the LA sample) evolution of the local tertiary structure away from the end point deoxy conformation. The direction of the conformational changes as reflected in both spectroscopic and kinetic markers is clearly toward that of higher affinity populations. The rapidity of the changes for the HA sample within the sol−gel makes it plausible that these initial changes are occurring within the boundary of the T state quaternary structure (with greatly weakened constraints). The spectroscopic markers clearly indicate that many of the constraints normally associated with the T state have been "loosened" as was observed for effector-free partially liganded Fe−Zn hybrid derivatives of HbA (*10*).

The finding of a tunable range of structural and functional liganded intermediates that appear to be within the umbrella of the overall T quaternary structure of HbA is consistent with results of work on β37 mutants of HbA (*59*, *61*, *62*) and FeZn hybrids of HbA (*10*) where the diliganded hybrids showed an effector-dependent progression of functional and conformational properties that were interpreted as evidence for a progression of liganded tertiary conformations within the T quaternary state. This is not inconsistent with the tertiary two-state allosteric model recently proposed by Eaton and co-workers (*13*), since such progression of functional and conformational properties could arise from changes in the relative population of t and r tertiary species within the T quaternary conformation (*63*).

CONCLUSIONS

In this study we have employed sol−gel encapsulation to lock in hemoglobin samples in their initial T state and then trigger a slow conformational relaxation initiated by CO binding. VRR and UVRR spectra show that only after CO ligation are the two populations HA and LA spectroscopically distinct, indicating conformational differences. CO rebinding kinetic measurements confirm that the HA and LA species are functionally distinct. The combined findings correlate well with the differences in oxygen affinity reported earlier (*8*). The data support the notion that the sample preparation protocols and other environmental factors such as the presence of allosteric effectors do not change the protein's initial conformation. Rather, they determine, after ligand binding, the rate at which the initial deoxy T state structure relaxes along a path that first includes the LA T population and later the HA T population. The time scale for the progression is determined by a balance between the ligation-initiated evolution toward liganded R and factors, such as allosteric effectors and the gel, that favor conformations that resemble the initially encapsulated deoxy T population. This conclusion can account for the oxygen affinity results since the sample that undergoes more conformational relaxation once oxygen binds will display a higher oxygen affinity.

REFERENCES

1. Eaton, W. A., Henry, E. R., Hofrichter, J., and Mozzarelli, A. (1999) Is cooperative oxygen binding by hemoglobin really understood? *Nat. Struct. Biol. 6*, 351−358.
2. Henry, E. R., Jones, C. M., Hofrichter, J., and Eaton, W. A. (1997) Can a two-state MWC allosteric model explain hemoglobin kinetics? *Biochemistry 36*, 6511−6528.
3. Monod, J., Wyman, J., and Changeux, J. P. (1965) On the nature of allosteric transitions: a plausible model, *J. Mol. Biol. 12*, 88−118.
4. Mueser, T. C., Rogers, P. H., and Arnone, A. (2000) Interface sliding as illustrated by the multiple quaternary structures of liganded hemoglobin, *Biochemistry 39*, 15353−15364.
5. Lukin, J. A., Kontaxis, G., Simplaceanu, V., Yuan, Y., Bax, A., and Ho, C. (2003) Quaternary structure of hemoglobin in solution, *Proc. Natl. Acad. Sci. U.S.A. 100*, 517−520.
6. Ackers, G. K., Dalessio, P. M., Lew, G. H., Daugherty, M. A., and Holt, J. M. (2002) Single residue modification of only one dimer within the hemoglobin tetramer reveals autonomous dimer function, *Proc. Natl. Acad. Sci. U.S.A. 99*, 9777−9782.
7. Ackers, G. K., Holt, J. M., Burgie, E. S., and Yarian, C. S. (2004) Analyzing intermediate state cooperativity in hemoglobin, *Methods Enzymol. 379*, 3−28.
8. Bruno, S., Bonaccio, M., Bettati, S., Rivetti, C., Viappiani, C., Abbruzzetti, S., and Mozzarelli, A. (2001) High and low oxygen affinity conformations of T state hemoglobin, *Protein Sci. 10*, 2401−2407.

9. Shibayama, N., and Saigo, S. (2001) Direct observation of two distinct affinity conformations in the T state human deoxyhemoglobin, *FEBS Lett. 492*, 50−53.
10. Samuni, U., Juszczak, L., Dantsker, D., Khan, I., Friedman, A. J., Perez-Gonzalez-de-Apodaca, J., Bruno, S., Hui, H. L., Colby, J. E., Karasik, E., Kwiatkowski, L. D., Mozzarelli, A., Noble, R. W., and Friedman, J. M. (2003) Functional and spectroscopic characterization of half-liganded iron-zinc hybrid hemoglobin: evidence for conformational plasticity within the T state, *Biochemistry 42*, 8272−8288.
11. Tsuneshige, A., Park, S., and Yonetani, T. (2002) Heterotropic effectors control the hemoglobin function by interacting with its T and R states—a new view on the principle of allostery, *Biophys. Chem. 98*, 49−63.
12. Yonetani, T., Park, S., Tsuneshige, A., Imai, K., and Kanaori, K. (2002) Global allostery model of hemoglobin: Modulation of O2-affinity, cooperativity, and Bohr effect by heterotropic allosteric effectors, *J. Biol. Chem. 277*, 34508−34520.
13. Henry, E. R., Bettati, S., Hofrichter, J., and Eaton, W. A. (2002) A tertiary two-state allosteric model for hemoglobin, *Biophys. Chem. 98*, 149−164.
14. Hofrichter, J., Henry, E. R., Sommer, J. H., Deutsch, R., Ikeda-Saito, M., Yonetani, T., and Eaton, W. A. (1985) Nanosecond optical spectra of iron−cobalt hybrid hemoglobins: geminate recombination, conformational changes, and intersubunit communication, *Biochemistry 24*, 2667−2679.
15. Ghelichkhani, E., Goldbeck, R. A., Lewis, J. W., and Kliger, D. S. (1996) Nanosecond time-resolved absorption studies of human oxyhemoglobin photolysis intermediates, *Biophys. J. 71*, 1596−1604.
16. Goldbeck, R. A., Paquette, S. J., Bjorling, S. C., and Kliger, D. S. (1996) Allosteric intermediates in hemoglobin. 2. Kinetic modeling of HbCO photolysis, *Biochemistry 35*, 8628−8639.
17. Esquerra, R. M., Goldbeck, R. A., Reaney, S. H., Batchelder, A. M., Wen, Y., Lewis, J. W., and Kliger, D. S. (2000) Multiple geminate ligand recombinations in human hemoglobin, *Biophys. J. 78*, 3227−3239.
18. Sassaroli, M., and Rousseau, D. L. (1987) Time dependence of near-infrared spectra of photodissociated hemoglobin and myoglobin, *Biochemistry 26*, 3092−3098.
19. Bjorling, S. C., Goldbeck, R. A., Paquette, S. J., Milder, S. J., and Kliger, D. S. (1996) Allosteric intermediates in hemoglobin. 1. Nanosecond time-resolved circular dichroism spectroscopy, *Biochemistry 35*, 8619−8627.
20. Scott, T. W., and Friedman, J. M. (1984) Tertiary-structure relaxation in hemoglobin: a transient raman study, *J. Am. Chem. Soc. 106*, 5677−5687.
21. Hu, X., Rodgers, K. R., Mukerji, I., and Spiro, T. G. (1999) New light on allostery: dynamic resonance Raman spectroscopy of hemoglobin kempsey, *Biochemistry 38*, 3462−3467.
22. Friedman, J. M. (1994) Time-resolved resonance Raman spectroscopy as probe of structure, dynamics, and reactivity in hemoglobin, *Methods Enzymol. 232*, 205−231.
23. Su, C., Park, Y. D., Liu, G., and Spiro, T. G. (1989) Hemoglobin T−R structure dynamics from simltaneous monitoring of tyrosine and tryptophan time resolved UV resonance Raman signals, *J. Am. Chem. Soc. 111*, 3457−3459.
24. Rodgers, K. R., and Spiro, T. G. (1994) Nanosecond dynamics of the R→T transition in hemoglobin: ultraviolet Raman studies, *Science 265*, 1697−1699.
25. Jayaraman, V., Rodgers, K. R., Mukerji, I., and Spiro, T. G. (1995) Hemoglobin allostery: resonance Raman spectroscopy of kinetic intermediates, *Science 269*, 1843−1848.
26. Avnir, D., Braun, S., Lev, O., and Ottolenghi, M. (1994) Enzymes and other proteins entrapped in sol-gel materials, *Chem. Mater. 6*, 1605−1614.
27. Ellerby, L. M., Nishida, C. R., Nishida, F., Yamanaka, S. A., Dunn, B., Valentine, J. S., and Zink, J. I. (1992) Encapsulation of proteins in transparent porous silicate glasses prepared by the sol-gel method, *Science 255*, 1113−1115.
28. Abbruzzetti, S., Viappiani, C., Bruno, S., Mozzarelli, A. (2001) Enhanced geminate ligand rebinding upon photo-dissociation of silica gel-embedded myoglobin-CO, *Chem. Phys. Lett. 346*, 430−436.
29. Samuni, U., Navati, M. S., Juszczak, L. J., Dantsker, D., Yang, M., and Friedman, J. M. (2000) Unfolding and refolding of sol-gel encapsulated carbonmonoxymyoglobin: An orchestrated spectroscopic study of intermediates and kinetics? *J. Phys. Chem. B 104*, 10802−10813.
30. Samuni, U., Dantsker, D., Khan, I., Friedman, A. J., Peterson, E., and Friedman, J. M. (2002) Spectroscopically and kinetically distinct conformational populations of sol-gel-encapsulated carbonmonoxy myoglobin. A comparison with hemoglobin, *J. Biol. Chem. 277*, 25783−25790.
31. Shibayama, N., and Saigo, S. (2003) Oxygen equilibrium properties of myoglobin locked in the liganded and unliganded conformations, *J. Am. Chem. Soc. 125*, 3780−3783.
32. Sottini, S., Viappiani, C., Ronda, L., Bettati, S., and Mozzarelli, A. (2004) CO rebinding kinetics to myoglobin- and R state hemoglobin- doped silica gels in the presence of glycerol, *J. Phys. Chem. B 108*, 8478−8484.
33. Bettati, S., and Mozzarelli, A. (1997) T state hemoglobin binds oxygen noncooperatively with allosteric effects of protons, inositol hexaphosphate, and chloride, *J. Biol. Chem. 272*, 32050−32055.
34. Das, T. K., Khan, I., Rousseau, D. L., and Friedman, J. M. (1999) Temperature-dependent quaternary state relaxation in sol-gel encapsulated hemoglobin, *Biospectroscopy 5* (Suppl.), 64−70.
35. Juszczak, L. J., and Friedman, J. M. (1999) UV resonance raman spectra of ligand binding intermediates of sol-gel encapsulated hemoglobin, *J. Biol. Chem. 274*, 30357−30360.
36. Khan, I., Shannon, C. F., Dantsker, D., Friedman, A. J., Perez-Gonzalez-de-Apodaca, J., and Friedman, J. M. (2000) Sol-gel trapping of functional intermediates of hemoglobin: geminate and bimolecular recombination studies, *Biochemistry 39*, 16099−16109.
37. Shibayama, N., and Saigo, S. (1995) Fixation of the quaternary structures of human adult haemoglobin by encapsulation in transparent porous silica gels, *J. Mol. Biol. 251*, 203−209.
38. Shibayama, N. (1999) Functional analysis of hemoglobin molecules locked in doubly liganded conformations, *J. Mol. Biol. 285*, 1383−1388.
39. Shibayama, N., and Saigo, S. (1999) Kinetics of the allosteric transition in hemoglobin within silicate sol-gels, *J. Am. Chem. Soc. 121*, 444−445.
40. Pioselli, B., Bettati, S., Demidkina, T. V., Zakomirdina, L. N., Phillips, R. S., and Mozzarelli, A. (2004) Tyrosine phenol lyase and tryptophan indole-lyase encapsulated in wet nanoporous silica gels: selective stabilization of tertiary conformations, *Protein Sci. 13*, 913−924.
41. Khan, I., Dantsker, D., Samuni, U., Friedman, A. J., Bonaventura, C., Manjula, B., Acharya, S. A., and Friedman, J. M. (2001) Beta 93 modified hemoglobin: kinetic and conformational consequences, *Biochemistry 40*, 7581−7592.
42. Abbruzzetti, S., Viappiani, C., Bruno, S., Bettati, S., Bonaccio., M., Mozzarelli, A. (2001) Functional characterization of heme proteins encapsulted in wet nanoporous silica gels, *J. Nanosci. Nanotechnol. 1*, 407−413.
43. Rivetti, C., Mozzarelli, A., Rossi, G. L., Henry, E. R., and Eaton, W. A. (1993) Oxygen binding by single crystals of hemoglobin, *Biochemistry 32*, 2888−2906.
44. Mozzarelli, A., Rivetti, C., Rossi, G. L., Eaton, W. A., and Henry, E. R. (1997) Allosteric effectors do not alter the oxygen affinity of hemoglobin crystals, *Protein Sci. 6*, 484−489.
45. Rousseau, D. L., and Friedman, J. M. (1988) in *Biological Applications of Raman Spectroscopy* (Spiro, T. G., Ed.) pp 133-215, John Wiley & Sons, New York.
46. Zhao, X., Chen, R., Raj, V., and Spiro, T. G. (2001) Assignment of the 1511 cm(-1) UV resonance Raman marker band of hemoglobin to tryptophan, *Biopolymers 62*, 158−162.
47. Nagai, M., Wajcman, H., Lahary, A., Nakatsukasa, T., Nagatomo, S., and Kitagawa, T. (1999) Quaternary structure sensitive tyrosine residues in human hemoglobin: UV resonance raman studies of mutants at alpha140, beta35, and beta145 tyrosine, *Biochemistry 38*, 1243−1251.
48. Nagai, M., Kaminaka, S., Ohba, Y., Nagai, Y., Mizutani, Y., and Kitagawa, T. (1995) Ultraviolet resonance Raman studies of quaternary structure of hemoglobin using a tryptophan beta 37 mutant, *J. Biol. Chem. 270*, 1636−1642.
49. Huang, S., Peterson, E. S., Ho, C., and Friedman, J. M. (1997) Quaternary structure sensitive tyrosine interactions in hemoglobin: a UV resonance Raman study of the double mutant rHb (beta99Asp→Asn, alpha42Tyr→Asp), *Biochemistry 36*, 6197−6206.
50. Lalezari, I., Lalezari, P., Poyart, C., Marden, M., Kister, J., Bohn, B., Fermi, G., and Perutz, M. F. (1990) New effectors of human hemoglobin: structure and function, *Biochemistry 29*, 1515−1523.
51. Samuni, U., Dantsker, D., Ray, A., Wittenberg, J. B., Wittenberg, B. A., Dewilde, S., Moens, L., Ouellet, Y., Guertin, M., and

Friedman, J. M. (2003) Kinetic modulation in carbonmonoxy derivatives of truncated hemoglobins: The role of distal heme pocket residues and extended apolar tunnel, *J. Biol. Chem. 278*, 27241−27250.

52. Dantsker, D., Samuni, U., Friedman, A. J., Yang, M., Ray, A., and Friedman, J. M. (2002) Geminate rebinding in trehalose-glass embedded myoglobins reveals residue specific control of intramolecular trajectories, *J. Mol. Biol. 13*, 239−251.
53. Hu, X., and Spiro, T. G. (1997) Tyrosine and tryptophan structure markers in hemoglobin ultraviolet resonance Raman spectra: mode assignments via subunit-specific isotope labeling of recombinant protein, *Biochemistry 36*, 15701−15712.
54. Juszczak, L. J., Fablet, C., Baudin-Creuza, V., Lesecq-Le Gall, S., Hirsch, R. E., Nagel, R. L., Friedman, J. M., and Pagnier, J. (2003) Conformational changes in hemoglobin S (betaE6V) imposed by mutation of the beta Glu7-beta Lys132 salt bridge and detected by UV resonance Raman spectroscopy, *J. Biol. Chem. 278*, 7257−7263.
55. Dave, B. C., Miller, J. M., Dunn, B., Valentine, J. S., and Zink, J. I. (1997) Encapsulation of proteins in bulk and thin film sol-gel matrices, *J. Sol-Gel Sci. Technol. 8*, 629−634.
56. Peterson, E. S., Shinder, R., Khan, I., Juczszak, L., Wang, J., Manjula, B., Acharya, S. A., Bonaventura, C., and Friedman, J. M. (2004) Domain-specific effector interactions within the central cavity of human adult hemoglobin in solution and in porous sol-gel matrices: evidence for long-range communication pathways, *Biochemistry 43*, 4832−4843.
57. Friedman, J. M., Scott, T. W., Stepnoski, R. A., Ikeda-Saito, M., and Yonetani, T. (1983) The iron-proximal histidine linkage and protein control of oxygen binding in hemoglobin. A transient Raman study, *J. Biol. Chem. 258*, 10564−10572.
58. Friedman, J. M. (1985) Structure, dynamics, and reactivity in hemoglobin, *Science 228*, 1273−1280.
59. Peterson, E. S., and Friedman, J. M. (1998) A possible allosteric communication pathway identified through a resonance Raman study of four β37 mutants of human hemoglobin A, *Biochemistry 37*, 4346−4357.
60. Huang, J., Juszczak, L. J., Peterson, E. S., Shannon, C. F., Yang, M., Huang, S., Vidugiris, G. V., and Friedman, J. M. (1999) The conformational and dynamic basis for ligand binding reactivity in hemoglobin Ypsilanti (beta 99 asp→Tyr): origin of the quaternary enhancement effect, *Biochemistry 38*, 4514−4525.
61. Kwiatkowski, L. D., Hui, H. L., Wierzba, A., Noble, R. W., Walder, R. Y., Peterson, E. S., Sligar, S. G., and Sanders, K. E. (1998) Preparation and kinetic characterization of a series of betaW37 variants of human hemoglobin A: evidence for high-affinity T quaternary structures, *Biochemistry 37*, 4325−4335.
62. Noble, R. W., Hui, H. L., Kwiatkowski, L. D., Paily, P., DeYoung, A., Wierzba, A., Colby, J. E., Bruno, S., and Mozzarelli, A. (2001) Mutational effects at the subunit interfaces of human hemoglobin: evidence for a unique sensitivity of the T quaternary state to changes in the hinge region of the alpha 1 beta 2 interface, *Biochemistry 40*, 12357−12368.
63. Viappiani, C., Bettati, S., Bruno, S., Ronda, L., Abbruzzetti, S., Mozzarelli, A., and Eaton, W. A. (2004) New insights into allosteric mechanisms from trapping unstable protein conformation in silica gels, *Proc. Natl. Acad. Sci. U.S.A.* (in press).

BI048531D